Annealed crystallization of ultrafine amorphous NiB alloy studied by XAFS

Shiqiang Wei[a,b], Zhongrui Li[a], Shilong Yin[c], Xinyi Zhang[a], Wenhan Liu[a,b], and Xiaoguang Wang[a]

[a]National Synchrotron Radiation Laboratory, University of Science and Technology of China, Hefei 230029,P.R.China, [b]Department of Astronomy and Applied Physics, University of Science and Technology of China, Hefei 230026, P.R.China, [c]Department of Mathematics and Physics, Hohai University, Nanjing 210024, P.R.China.
E-mail: sqwei@ustc.edu.cn

XAFS has been used to investigate the local structure evolutions of ultrafine amorphous NiB alloy during the annealed crystallization process. A nanocrystalline Ni phase with the local structure of crystalline Ni-like and a crystalline Ni_3B, have been produced for ultrafine amorphous NiB alloy under the annealed temperature of 573 K. The results rule out Rojo *et al.*'s devitrification mechanism of $Ni_{80}B_{20}$ amorphous alloy in which they considered that an amorphous pure Ni phase is formed in the first exothermic process. However, our results are almost identical with Riveiro *et al.*'s conclusion in which the intermediate state is interpreted as two metastable crystalline phases of Ni_3B and Ni-rich NiB alloy. With the annealed temperature going onto 773 K, the ultrafine NiB sample is further decomposed and crystallized into crystalline Ni with long-range order.

Keywords: XAFS, DTA, ultrafine amorphous NiB alloy.

1. Introduction

Ultrafine amorphous NiB alloy has attracted special attention in view of its unique physical and chemical properties (Linderoth and Morup, 1991; Chen *et al*., 1998; Liebermann, 1993). For example, ultrafine amorphous particles have such advantages that they may be compacted to any shape, suspended in a liquid to make ferrofluid, and used for catalysis and magnetic recording applications (Hu *et. al*., 1999; Ma *et al*., 1997). In order to understand the nature of ultafine amorphous NiB alloy, a number of work were focused on studying their structures, stability and performances (Egami *et al*., 1984; Liebs *et al*., 1995; Yu *et al*., 1994; Saida *et al.*, 1991; *Li et al*., 1998).

Recently, Rojo *et al.* (1996) have reported that annealing an amorphous $Ni_{80}B_{20}$ alloy results in an intermediate state which is nanocrystalline with Ni_3B crystallites surrounded by an amorphous pure Ni phase, based on the calorimetric, x-ray diffraction (XRD) and magnetic measurements. On the contrary, Riveiro *et al.* (1998) have explained the broad shoulder superimposed on the Ni_3B peaks as a consequence of overlapping of broad x-ray peaks produced by nanocrystals, using the Rietveld refinement method. More recently, the theoretical calculation by Somoza and Gallego (2000) has considered that Riveiro *et al*.'s result is the more plausible account of the devitrification of $Ni_{80}B_{20}$ glass. These conclusions were mainly deduced from XRD, magnetic and resistance measurements. In fact, it is very difficult to obtain the local structure from atomic level structural determination by XRD for a material with short-range order, since XRD can only give information on long-range order structure and lattice strain. In this work, XAFS was used to investigate the local structure evolutions of ultrafine amorphous NiB alloy during the annealed crystallization process.

2. Experiments

The preparation of ultrafine amorphous $Ni_{70}B_{30}$ alloy powder is described elsewhere (Shen *et al.*, 1997; Wei *et al.*, 2000). The annealed crystallization procedures of ultrafine amorphous NiB alloy are as follows. First, as-prepared NiB powder of 2g was placed in a pipe furnace, and then flow with a high purity Ar gas. Second, the sample was slowly elevated to the annealed temperature designed in advance, and was kept at the temperature for 2h. Finally, the annealed NiB sample can be obtained after it was naturally cooled down to room temperature.

The X-ray absorption spectra at Ni K-edge for the as-prepared and annealed $Ni_{70}B_{30}$ samples were measured at the beamline of U7C of National Synchrotron Radiation Laboratory (NSRL) and the beamline of 4W1B of Beijing Synchrotron Radiation Facility (BSRF). The storage ring of NSRL was operated at 0.8 GeV with a maximum current of 160 mA, and the hard x-ray beam is from a three-pole superconducting wiggler with a magnetic field intensity of 6 Tesla. The storage ring of BSRF was run at 2.2 GeV with a maximum current of 100 mA. The XAFS spectra of NSRL were recorded in transmission mode with ionization chambers filled with Ar/N_2 at room temperature, by using Keithley Model 6517 Electrometer to collect the electron charge directly. XAFS Data were analyzed by USTCXAFS1 soft package compiled by Wan and Wei and UWXAFS3.0 software package according to the standard procedures (Wan and Wei, 1999; Stern *et al.*, 1995; Sayers *et al.*, 1988).

The differential thermal analysis (DTA) profile of ultrafine amorphous NiB alloy powder was performed using CDR-1 differential thermal analysis-meter (Shanghai Balance Co.). The samples were heated from room temperature to 873 K with a heating rate of 10 K min^{-1} in a flow of Ar gas of 30 ml min^{-1} at ambient pressure.

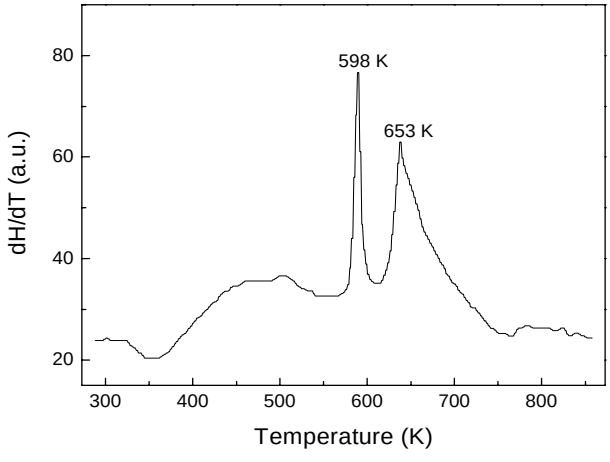

Figure 1
DTA profile of ultrafine amorphous NiB alloy

3. Results and Discussions

The thermal evolutions of ultrafine amorphous NiB alloy in the temperature region between 298 and 873 K are shown in Fig. 1. It can be observed that there are two stronger exothermic peaks in

the DTA profiles of ultrafine amorphous NiB alloy. The first peak located at 598 K is very sharp and the second peak located at 653 K is rather broad. Moreover, the area of the second peak is about twice as large as that of the first one. After the annealed temperature being elevated to 873 K, no new exothermic peak appears.

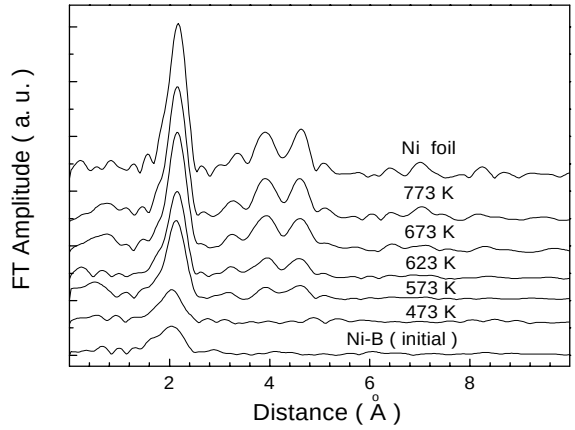

Figure 2
RDFs of ultrafine amorphous NiB alloy

The radial distribution functions (RDF) of NiB sample at differently annealed temperatures, obtained from their $\chi(k)k^3$ by fast Fourier transform, were displayed in Fig. 2. There is only one prominent magnitude peak in the first nearest neighbor of Ni atoms for the as-prepared NiB sample and the one annealed at 473 K. The result clearly indicates that the local structures around Ni atoms show an amorphous feature for these NiB samples. After being annealed at 573 K, the intensity of the first magnitude peak of NiB sample was significantly enhanced, and the second and third magnitude peaks appear at the position of 4.0 and 4.6 Å, respectively. The shape feature of RDF curve of NiB sample annealed at 573 K is the same as that of Ni foil despite the magnitude intensity is about 40% lower. The result implies that the local structure around Ni atoms in the NiB sample annealed at 573 K is similar to that of Ni foil. However, no peaks corresponding to Ni phase can be found in the XRD patterns (Wei *et al.*, 2000). In order to well understand the local structures of the as prepared and annealed NiB samples, the RDFs of crystalline Ni (c-Ni) and Ni_3B (c-Ni_3B) calculated by FEFF7 software package (Rehr *et al*., 1992) are demonstrated in Fig. 3 for comparison. It can be observed that the RDF shape of c-Ni_3B are evidently different from that of c-Ni, and the magnitude intensity of the first main peak of c-Ni_3B is much lower, only about one fourth as high as that of c-Ni. Therefore, the intensity and shape of RDF curve for NiB sample annealed at 573 K can not only be explained by the formation of c-Ni_3B, but also have to include the nanocrystalline Ni. For the NiB sample annealed at 773 K, its RDF shape and intensity are almost the same as those of Ni foil. It suggests that the highly annealed temperature can drive NiB sample to form crystalline Ni particles with long-range order.

In order to get structural parameters of the first nearest neighbor shell of Ni atoms of NiB sample, the high-frequency noise and the small residual background must be removed. The RDF was inversely transformed to isolate the single shell EXAFS contribution. The least-squares minimization technique, based on Marquart's scheme for iterative estimation of nonlinear least-squares parameters via a compromise combination of gradient and Taylor series method (Sayers *et al.*, 1988) was used to fit the inverse transform EXAFS spectra. For the amorphous NiB alloy, the asymmetric pair distribution function $G(R)_{asym}$ was assumed as a convolution of Gaussian function P_G, with a Debye waller factor σ_T and exponential function P_E, with an assymetric coefficient σ_S. The EXAFS formula has been shown elsewhere (Wu *et al.*, 1997; Prouzet *et al.*, 1997; Wei *et al.*, 2000). The theoretical amplitude function $|F_j(k,\pi)|$ and phase shift function $\Phi_{ij}(k)$ obtained by FEFF7 (Rehr *et al.*, 1992) were used to fit the XAFS data of ultrafine amorphous NiB alloy. The results of curve fitting are summarized in Table 1

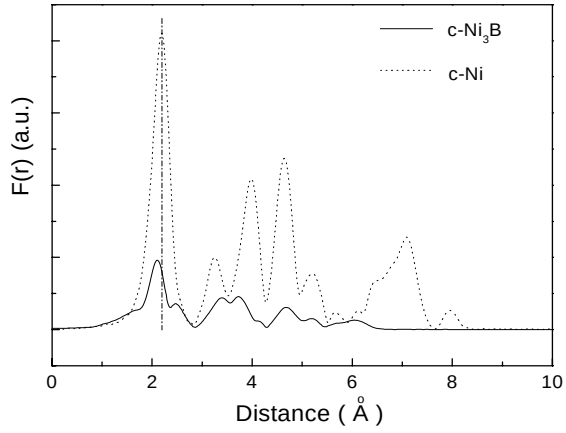

Figure 3
RDFs of c-Ni and c-Ni_3B calculated from FEFF7 software package

Table 1
The structure parameters of ultrafine amorphous NiB alloy at different annealing temperature

Sample	temp K	pair	R_j (Å)	R_0 (Å)	N	σ_T (10^{-2} Å)	σ_S (10^{-2} Å)	ΔE_0 (eV)
NiB	298	Ni-Ni	2.75	2.41± 0.02	11.0± 1.0	6.9	33	-0.2
		Ni-B	2.18	2.15± 0.02	2.7± 0.2	4.6	3.4	-4.7
NiB	573	Ni-Ni	2.55	2.43± 0.02	9.9± 1.0	6.0	11	-0.9
		Ni-B	2.18	2.15± 0.02	2.6± 0.2	6.0	2.9	5.0
NiB	773	Ni-Ni	2.49	2.45± 0.02	10.8± 1.0	7.0	2.9	1.6
		Ni-B	2.17	2.15± 0.02	0.3±0.2	5.6	2.3	-5.0
Ni foil		Ni-Ni	2.49		12.0	7.4		

Average distance $R_j = R_0 + \sigma_S$, error bar of R = ±0.02 Å, error bar of σ_T = ± 0.5×10^{-2} Å error bar of σ_S = ±1×10^{-2} Å.

The XAFS results in table 1 quantitatively indicate that the average bond length R_j, coordination number N, thermal disorder σ_T and the assymetric disorder factor σ_S are 2.75 Å, 11.0, 0.069 Å and 0.33 Å for the first neighbor Ni-Ni shell of the as-prepared ultrafine amorphous NiB alloy, respectively. After annealed at 573 K, ultrafine amorphous NiB alloy starts to be crystallized. Its R_j and σ_S of Ni-Ni shell decrease notably from 2.75 to 2.55 Å and from 0.33 to 0.11 Å, respectively. The results evidently demonstrated that the local structure of NiB sample annealed at 573 K is close to that of Ni foil. Furthermore, the RDF curve shown in Fig. 2 indicates that the local structure of NiB sample annealed at 573 K is crystalline Ni-like. The XAFS results have revealed that a nanocrystalline Ni phase with small particle size is formed for the NiB sample annealed at 573 K, despite no

diffraction peak of crystalline Ni appears in its XRD pattern (Wei *et al*., 2000). If only crystalline Ni_3B is produced in the first exothermic process, the RDF intensity of NiB sample annealed at 573 K should be much lower, just as the RDF intensity of crystalline Ni_3B in Fig. 3. This result is in good agreement with Riveiro *et al*.'s results (Riveiro *et al.*, 1998). Riveiro *et al*. have considered that the devitrification of amorphous $Ni_{80}B_{20}$ alloy into Ni_3B and crystalline Ni occurs in a single step, indicated by their electric and magnetic measurements where the electrical resistance keeps nearly constant after the first exothermic process (Riveiro *et al.*, 1998). The intermediate state is composed of two crystalline phases, one is a Ni_3B structure with excess Ni and the other is a Ni-rich NiB alloy in which atomic concentration of B is lower than 5%. Our results rule out Rojo *et al*.'s conclusion (Rojo *et al.*, 1996), in which they considered not only crystalline Ni_3B but also an amorphous pure Ni phase was formed after the crystallization at 573 K, in the first exothermic process. After annealed at 773 K, the structural parameters of NiB sample were almost the same as those of Ni foil. In particular, the σ_S of Ni-Ni shell of NiB sample decreases to a small value of 0.029 Å. The result means that most of NiB has been decomposed into crystalline Ni.

Summarized above DTA and XAFS results as shown in Fig. 1 and Fig. 2, it is easy to obtain this conclusion that the crystallization process of ultrafine amorphous NiB alloy is in two steps. After the first exothermic process at the annealed temperature of 573 and 623 K, both of nanocrystalline Ni and c–Ni_3B are formed. When the annealed temperature is higher than that of second exothermic peak of 653 K, the RDF shape of the annealed NiB sample is similar to that of crystalline Ni foil. The result indicates that the ultrafine amorphous NiB alloy can be crystallized to form crystalline Ni powder under the higher temperature.

Acknowledgments

This research work was supported by "100 people plan" and "9·5 programs" of Chinese Academy of Sciences.

References

Ballesteros, C., Zern, A., Garcia-Escorial, A., Hernando, A. & Rojo, J. M., (1998). *Phys. Rev. B.* **58**, 89.

Chen, Y., (1998). *Catalysis Today*. 44, 3.

Crozier, E.D. , (1995). *Physica B.* **208&20**9, 330.

Crozier, E.D., Rehr, J.J. & Ingalls, R., (1988). *X-ray Absorption, Principles, Applications, Techniques of EXAFS, SEXAFS and XANES*, P.373, edited by Koningsberger, D.C., and Prins,R., John Wiley and Sons, Inc.

Deng, J.F., Yang, J., Sheng, S.S., Chen, H.R., Xiong, G.X., (1994). *J. Catal.* **150**, 434.

Egami, T. & Waseda, Y., (1984). *J. Non-crystal. Solids*. **64**, 113.

Gutierrez, A. & Lopez, M. F., Hernando, A., Rojo, J. M., (1997). *Phys. Rev. B.* 56, 5039.

Hu, Z., Fan, Y. & Chen, Y., (1999). *Appl. Phys. A.* 68, 225.

Li, H.X., Chen, H.Y., Dong, S.Z., Yang, J.S. & Deng, J.F., (1998). *Appl. Surf. Sci.* 125, 115.

Li, T.X., Zhang, X.F., Li, H.Q., Jin, C.D., Jiang, Y.L., Cui, J.T., Wang, D.Q., (1995). *Chinese J. Catal.* 16, 299.

Liebermann, H.H, Rapidly Solidified alloys, (1993) M. Dekker, New York.

Liebs, M., Hummler, K. & Fahnle, M., (1995). *Phys. Rev. B.* 51, 8664.

Linderoth, S. & Morup, S., (1991). *J. Appl. Phys.* **69**, 5256.

Ma, L., Huang, W., Yang, J. & Deng, J.F., (1997). *J. Phys. IV*. **7** (C2), 909.

Prouzet, E., Michalowicz, A., Allali, N., (1997). *J. Phys. IV,* **7**, C2-261.

Rehr, J.J., Zabinsky, S.I.& Albers, R.C., (1992). *Phys. Rev. Lett.* **69**, 3397.

Riveiro, J. M. & Muniz, P., (1998). *Phys. Rev. B.* **58**, 11093.

Riveiro, J.M., Muniz, P., Andres, J.P., Lopez de la Torre, M.A., (1998). *J. Magn. Magn. Mater.* **188**, 153.

Rojo, J.M., Hernando, A., Ghannami, M.EI., Garcia-Escorial, A., Gonzalez, M.A., Garcia-Martinez, R. & Ricciarelli, L., (1996). *Phys. Rev. Lett.* **76**, 4833.

Sayers, D. E., & Bunker, B. A., (1988). *X-ray Absorption, Principles, Applications, Techniques of EXAFS, SEXAFS and XANES*, P.211, edited by Koningsberger, D.C., and Prins,R., John Wiley and Sons, Inc.

Saida, J., Inoue, A. & Masumoto, T., (1991). *Mater. Sci. Eng. A.* 133, 771.

Shen, B.R., Wei, S.Q., Fan, K.N., and Deng, J.F., (1997). *Appl.phys. A*, **65**, 295.

Somoza, J.A. & Gallego, L.J., (2000). *Phys.Rev. B.* **61**, 3177.

Stern, E.A., Newville, M., Ravel, B., Yacoby, Y. & Haskel, D., *UWXAFS3.0 Software Package* (1995).

Wan, X.H. Wei, S. Q. *USTCXAFS 1.0 Software Package* (May 1999).

Wei, S.Q., Chen, C.R., Bian, G.Z., Li, Z.R., Liu, W.H., and Zhang, X.Y., (2000). *Chinese Science Abstracts.* **6**, 113.

Wei, S.Q., Oyanagi, H., Liu, W.H., Hu, T.D., Yin, S.L. & Bian, G.Z., (2000). *J. non-crystalline Solids*. **275**, 160.

Wu, L.W., Wei, S.Q., Wang, B. & Liu, W.H., (1997). *J.Phys. CM*, **9**, 3521.

Yu, M. and Kakehashi, Y., (1994). *Phys. Rev. B.* **49**, 15723.